SPECIAL SECTION: OVARIAN CANCER

Intra- and peritumoral radiomics for predicting early recurrence in patients with high-grade serous ovarian cancer

Yujiao Wu[1] · Wenyan Jiang[2] · Langyuan Fu[1] · Meihong Ren[1] · Hua Ai[1] · Xingling Wang[3]

Abstract

Purpose To explore values of intra- and peritumoral CT-based radiomics for predicting recurrence in high-grade serous ovarian cancer (HGSOC) patients.

Methods This study enrolled 110 HGSOC patients from our hospital between Aug 2017 and Apr 2021. All patients underwent contrast-enhanced CT scans before treatment. The least absolute shrinkage and selection operator (LASSO) regression was used to select radiomics features from intra- and peritumoral areas. Radiomics signatures were built based on selected features from Intra-RS, Peri-RS, and in Com-RS. A nomogram was constructed by combining radiomics signatures and clinical parameters with predictive potential. Receiver operating characteristics (ROC), calibration, and decision curve analyses (DCA) curves were used to evaluate performance of the nomogram.

Results The intra- and peritumoral combined Com-RS showed effective ability in predicting recurrent HGSOC in the training (AUCs, Intra-RS vs. Peri-RS vs. Com-RS, 0.861 vs. 0.836 vs. 899) and validation (AUCs, Intra-RS vs. Peri-RS vs. Com-RS, 0.788 vs. 0.762 vs. 815) cohort. The Federation of International of FIGO stage, menstruation, and location were found to be strongly associated with tumor recurrence. The nomogram has the best predictive ability in the training (AUCs, Com-RS vs. clinical model vs. nomogram, 0.899 vs. 0.648 vs. 0.901) and validation (AUCs, Com-RS vs. clinical model vs. nomogram, 0.815 vs. 0.666 vs. 0.818) cohort.

Conclusion Our findings suggested values of intra- and peritumoral-based radiomics for predicting recurrent HGSOC. The constructed nomogram may be of importance in clinical application.

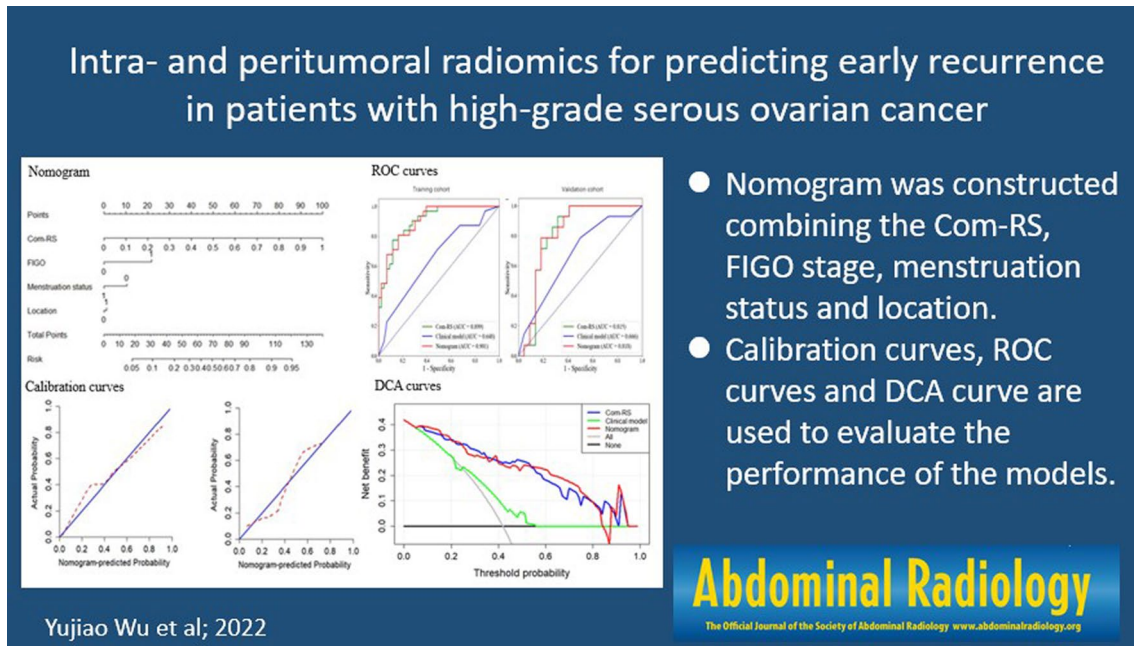Yujiao Wu and Wenyan Jiang have contributed equally to this work.

✉ Xingling Wang
  wangxingling@cancerhosp-ln-cmu.com

1 Department of Biomedical Engineering, School of Intelligent Medicine, China Medical University, Shenyang 110122, People's Republic of China

2 Department of Scientific Research and Academic, Liaoning Cancer Hospital and Institute, Cancer Hospital of China Medical University, Shenyang 110042, People's Republic of China

3 Department of Gynecology, Liaoning Cancer Hospital and Institute, Cancer Hospital of China Medical University, Shenyang 110042, People's Republic of China

Graphical Abstract

Intra- and peritumoral radiomics for predicting early recurrence in patients with high-grade serous ovarian cancer

- Nomogram was constructed combining the Com-RS, FIGO stage, menstruation status and location.
- Calibration curves, ROC curves and DCA curve are used to evaluate the performance of the models.

Yujiao Wu et al; 2022

Introduction

Ovarian cancer (OC) has been the deadliest cancer among women and the second most common gynecological malignancy worldwide [1]. Epithelial ovarian cancer (EOC) is the most common type of OC, and HGSOC accounts for 75% of all EOC which is the most represented in the prognostic studies of OC [2]. The prognosis of patients with HGSOC is poor because of high recurrence rate, and the median recurrence time of advanced stage HGSOC is usually less than 18 months [3, 4]. Clinical reports have shown that a proportion of HGSOC patients obtain a good postoperative response after receiving cytoreductive surgery and platinum-based chemotherapy [5, 6]. However, postoperative recurrence rates for advanced (stage III or IV) and early stage (stage I or II) HGSOC have been reported to be 60–80% and 20–25%, respectively [7]. Therefore, an effective method for pretreatment assessing and predicting the risk of cancer recurrence for HGSOC is of clinical importance to develop follow-up treatment plans and improve prognosis. The role of medical imaging technologies in HGSOC patients is fast evolving in recent years [8]. The contrast-enhanced computed tomography (CT) is routinely clinically used for staging and evaluating treatment follow-up in HGSOC [7]. However, radiologists can still hardly predict patients' responses or prognosis by visual inspection of pretreatment CT images due to the absence of predictive biomarker.

Radiomics is an emerging field in quantitative medical imaging for objectively describing tumor characteristics and phenotypes [9]. In recent years, the radiomics have been introduced to reveal quantitative predictive or prognostic associations between images and clinical outcomes by capturing and selecting important imaging-based features [10]. There have been many radiomics approaches on HGSOC, which have confirmed that medical images contain a wealth of potential information that is relevant to prognosis of patients [11–13]. A recent study showed that radiomics features derived from magnetic resonance imaging images were correlated with prognosis of HGSOC [14]. Another recent report suggested significant associations between CT-based features and the risk of disease progression [15].

However, previous studies only focused on intratumoral area and ignored values of peritumoral area of HGSOC, which have inherent limitations. Pathological studies have demonstrated that peritumoral stroma surrounding HGSOC may also hold great biological information related to distinct biological characteristics of the tumor [16, 17]. Peritumoral radiomics has also been proofed to increase the efficiency of the prediction for the risk of recurrence in many types of malignant tumors, such as lung cancer [18], intrahepatic cholangiocarcinoma [19], and colorectal cancer [20]. To our knowledge, peritumroral radiomics for predicting recurrent HGSOC have not been studied. We hypothesized that peritumoral regions of HGSOC seen on CT images could

hold potential biomarkers to cancer recurrence, and merits investigation. The study enrolled patients with HGSOC, aiming to explore values of CT-based features for predicting recurrence in these patients. We aim to analyze both intra- and peritumoral areas of HGSOC and develop a radiomics-clinical nomogram that may have potential applications to provide personalized treatment for patients with HGSOC.

Materials and methods

Patients

This retrospective study was approved by our institutional review committee. A total of 110 HGSOC patients were recruited between Aug 2017 and Apr 2021. The inclusion criteria were as follows: (1) patients were pathologically confirmed as HGSOC and treated with cytoreductive surgery and 6–8 cycles of platinum-based chemotherapy; (2) patients aged 18–70 years; (3) with complete follow-up (disease history, procedure and course records, etc.), clinical and pathological information; and (4) received contrast-enhanced CT scans before surgery. The exclusion criteria were as follows: (1) with other tumor diseases; (2) received other treatments, including preoperative chemotherapy, neoadjuvant chemotherapy, or immunotherapy; and (3) poor quality of preoperative CT images. The patient screening process is summarized in Fig. 1. The final patients included in the experiment were randomly divided into a training cohort (n = 74) and a test cohort (n = 36) in a 2:1 ratio. Clinical characteristics

of patients including age, Federation of International of Gynecologists and Obstetricians (FIGO), preoperative carbohydrate antigen 125 (CA125), menstruation status, tumor side, and tumor diameter were collected by reviewing medical records and CT images.

Follow-up and clinical endpoints

The follow-up period in our study is 12 to 24 months. The PFS was defined as the time interval between the date of surgery to the date of disease recurrence or end of follow-up. Clinical endpoint is disease recurrence or progression. Follow-up data are obtained from two main sources: medical records and telephone inquiries by physicians. CA125 elevation above normal range and abnormal CT images are considered as cancer recurrence.

Imaging acquisition and tumor segmentation

Patient's contrast-enhanced CT data were obtained from a Siemens CT scanner (Magnetom V erioio, Erlangen). The scanning parameters were as follows: tube voltage, 120 kVp; tube current, 350 mA; slice thickness, 5 mm; slice spacing, 5 mm; matrix, 512×512; rotating speed, 0.5 s/rot; and contrast medium, 80–100 mL injector rate, 2.5–3.5 mL/s. Arterial and portal vein enhancement scans were performed 25 s and 70 s after the contrast injection. The scanned full enhanced CT images were stored in digital imaging and communications in medicine (DICOM) format. A radiologist with 17 years of experience used
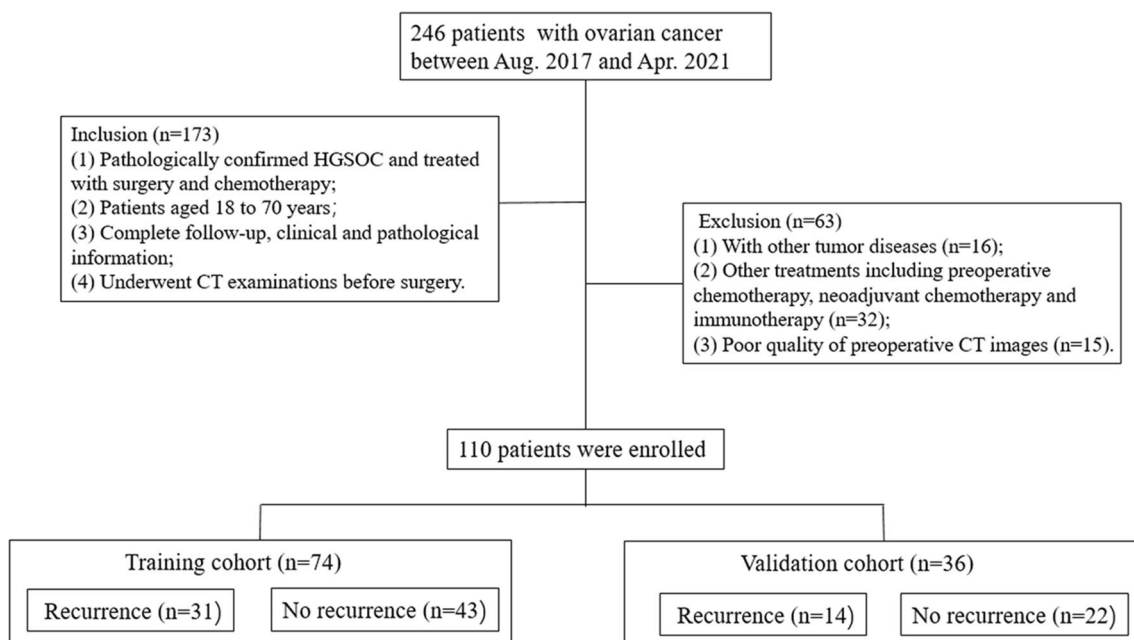

Fig. 1 Flowchart of the patient screening process in our study

the open source software ITK-SNAP V.3.8 to manually delineate the region of interest (ROI) on each CT slice to generate the mask and stored in a NII format. To explore potential information in the peritumoral region of ovarian cancer, the original mask of the tumor were radially dilated with a distance of 1 cm outside the tumor using Python v.3.6. The ROI of the peritumoral region was obtained by subtracting the original ROI from the dilated ROI.

Extraction and selection of radiomics features

Radiomics features for each patient were calculated from both intra- and peritumoral regions using the "Pyradiomics" package in Python v.3.6 (https://pyradiomics.readthedocs.io) [21]. Eight transform filters (wavelet, square, squareroot, localbinarypattern2D, Laplacian of Gaussian, logarithm, exponential, and gradient) were required for the CT images. In total, 1967 features were extracted from the intratumoral and peritumoral regions, respectively. These include three major categories: first order, shape based, and texture features. In addition, all texture features extracted are shown in Table S1. Among them, the first order and texture features were derived from the transformed CT images.

To evaluate the reliability of the extracted features and to exclude unstable features, 30 patients were randomly selected for intra-class correlation coefficient (ICC) analysis [22], 15 patients had disease recurrence, and the other 15 patients were without disease recurrence during the follow-up period. To perform the ICC analysis, another radiologist with 2-year experience was invited to segment the ROIs in the CT image. Features with ICC > 0.85 were retained and further selected by three steps. First, the Mann–Whitney U test was used to select features with $P < 0.05$. Second, the least absolute shrinkage and selection operator (LASSO) regression and tenfold cross-validation are used to select features with the best predictive performance, and lambda is the best parameter chosen by LASSO and tenfold cross-validation [23]. Finally, logistic regression of the remaining features using Akaike information criterion (AIC) as a stopping criterion [24].

Development of radiomics signatures and nomogram

The radiomics signature was developed by integrating the selected features with non-zero coefficients based on LASSO regression. To help clinicians predict disease recurrence in ovarian cancer patients, a radiomics nomogram was constructed by combining the radiomics signature with most important clinical factors.

Statistical analysis

For categorical and continuous clinical factors, the Chi-square [25] and Mann–Whitney U tests [26] were applied for statistical analysis using IBM SPSS Statistics 24. Clinical factors with $P > 0.05$ were excluded and not used for modeling. Receiver operating characteristic (ROC) curves were plotted using the "pROC" package in R v.3.6 and optimal cutoff values were calculated using Youden index [27]. The area under the ROC curve (AUC), accuracy, sensitivity, and specificity as metrics were calculated to evaluate predictive performance of the radiomics models. ROC curves were evaluated with the DeLong test [28]. Decision curves (DCA) [29] were plotted using the "rms" package for assessing potential clinical values of the models. Figure 2 shows the workflow of our study.
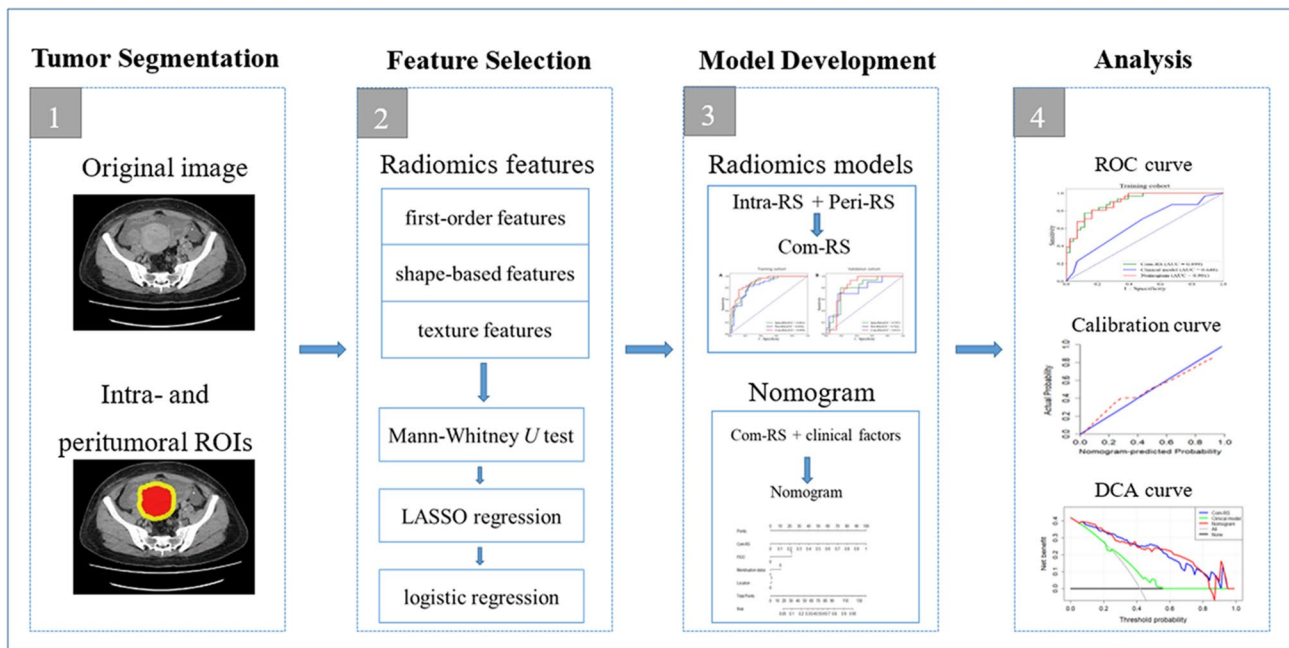
Results

Patient characteristics

We finally enrolled 110 patients with HGSOC: mean age, 53.65 ± 10.18 years. Significant differences were observed in FIGO Stage, menstruation, and location between recurrence and no recurrence groups in the training set ($P < 0.05$); the differences were later confirmed in the validation set as well ($P < 0.05$). There was no difference observed for age and tumor diameter ($P > 0.05$), except for preoperative CA125 that showed $P < 0.05$ in the training set. Results of statistical analysis of clinical characteristics are listed in Table 1.

Feature selection and development of radiomics signatures

The ICC, Mann–Whitney U test, and LASSO regression were used to select CT-based radiomics features that were most strongly associated with recurrence of HGSOC patients. A total of five and four CT features were selected from intra- and peritumoral areas to generate an intratumoral area (Intra-RS) and a peritumoral area (Peri-RS), respectively. The features from intra- and peritumoral areas were combined and further selected to generate a combined radiomics signature (Com-RS) with six most predictive features, four from intra-, and two from peritumoral areas, respectively. Predictive performance of the finally identified features is compared and presented in Table 2. Formulas of the developed radiomics signatures are shown below:

Intra-RS = 4.831–26.367 × log.sigma.5.0.mm.3D_glszm_SizeZoneNonUniformityNormalized − 4.717 × original_shape_Flatness + 4.726 × wavelet-

Fig. 2 Radiomics workflow in our study

Table 1 Statistical analysis results of clinical characteristics

Characteristic	Training (n = 74)		P	Validation (n = 36)		P
	Recurrence (n = 31)	No recurrence (n = 43)		Recurrence (n = 14)	No recurrence (n = 22)	
Age (mean ± SD)	54.00 ± 9.19	52.74 ± 9.88	0.662	56.71 ± 10.45	52.95 ± 12.05	0.665
Pre-CA125 (median (range))	936.00 (60.30, 7038.20)	317.30 (9.30, 8790.10)	0.005*	622.10 (121.90, 4578.60)	642.60 (7.70, 5551.20)	0.810
Tumor diameter (mean ± SD)	85.78 ± 22.00	87.52 ± 26.93	0.930	83.95 ± 26.31	86.34 ± 36.15	0.810
FIGO Stage, n. (%)						
Stage I–II	4 (5.41)	20 (27.03)	0.003*	1 (2.78)	8 (22.22)	0.003*
Stage III–IV	27 (36.49)	23 (31.08)		13 (36.11)	14 (38.89)	
Menstruation status, n. (%)						
Menopause	24 (32.43)	33 (44.60)	< 0.001*	12 (33.33)	19 (52.78)	< 0.001*
Premenopausal	7 (9.46)	10 (13.51)		2 (5.56)	3 (8.33)	
Location, n. (%)						
Unilateral	10 (13.51)	16 (21.62)	0.011*	3 (8.33)	8 (22.22)	0.020*
Bilateral	21 (28.38)	27 (36.49)		11 (30.56)	14 (38.89)	

SD standard deviation, *FIGO* Federation of International of Gynecologists and Obstetricians, *Pre-CA125* preoperative carbohydrate antigen 125

*$P < 0.05$

LLH_glszm_LowGrayLevelZoneEmphasis − 0.105 × wavelet-LHH_firstorder_Kurtosis − 2.198 × log. sigma.3.0.mm.3D_glcm_ClusterShade

Peri-RS = 2.355 + 3.327 × square_glcm_MCC − 0.595 × logarithm_glszm_ZoneEntropy − 5.052E − 07 × wavelet-HLL_glszm_LargeAreaLowGrayLevelEmphasis − 4.144 × original_shape_Flatness

Com-RS = 5.655–7.544 × original_shape_Flatness − 0.099 × wavelet-LHH_firstorder_Kurtosis − 24.370 × log.sigma.5.0 mm.3D_glszm_SizeZoneNonUniformityNormalized − 3.155 × log.sigma.3.0 mm.3D_glcm_ClusterShade − 1.138E-06 × wavelet-HLL_glszm_LargeAreaLowGrayLevelEmphasi + 5.025 × wavelet-LLH_glszm_LowGrayLevelZoneEmphasis.

Table 2 Performance of the features for predicting recurrent OC

Feature	Region	Cohort	Mean ± SD		AUC	P
			Recurrence	No recurrence		
Wavelet.LHH_firstorder_Kurtosis	Intra	Training	5.30 ± 3.50	10.83 ± 12.42	0.695	0.004
		Validation	7.06 ± 9.78	18.28 ± 29.11	0.662	0.109
Log.sigma.5.0.mm.3D_glszm_Size-ZoneNonUniformi-tyNormalized	Intra	Training	0.10 ± 0.03	0.12 ± 0.04	0.647	0.032
		Validation	0.11 ± 0.07	0.12 ± 0.06	0.655	0.395
Log.sigma.3.0.mm.3D_glcm_Clust-erShade	Intra	Training	0.08 ± 0.24	0.20 ± 0.20	0.519	0.024
		Validation	0.14 ± 0.24	0.18 ± 0.18	0.699	0.860
Wavelet.LLH_glszm_LowGrayLeve-ZoneEmphasis	Intra	Training	0.23 ± 0.22	0.13 ± 0.14	0.642	0.038
		Validation	0.18 ± 0.13	0.14 ± 0.19	0.705	0.041
Original_shape_Flatness	Peri	Training	0.20 ± 0.10	0.31 ± 0.16	0.742	< 0.001
		Validation	0.23 ± 0.10	0.40 ± 0.21	0.740	0.016
Wavelet.HLL_glszm_LargeAreaLo-wGrayLevelEmpha-sis	Peri	Training	$6.10 \times 10^5 \pm 5.84 \times 10^5$	$1.48 \times 10^6 \pm 1.84 \times 10^6$	0.643	0.037
		Validation	$8.61 \times 10^5 \pm 7.39 \times 10^5$	$1.40 \times 10^6 \pm 1.56 \times 10^6$	0.558	0.575

SD standard deviation, *Intra*, intratumoral, *Peri* peritumoral

Table 3 lists comparisons of predictive performance for each radiomics signature. Our developed Intra-RS from the intratumoral area outperformed Peri-RS from the peritumoral area in terms of AUC and specificity in both training and validation cohorts. The intra- and peritumoral area combined Com-RS achieved the highest AUC in training and validation cohorts, indicating that the intra- and peritumoral areas may provide complementary information correlated to recurrence. Figure 3 shows waterfall plots for each patient based on the multi-area combined model. In waterfall plots, most patients can be correctly distinguished according to Com-RS in both training and validation cohorts, which suggests that our model is effective on differentiating patients with recurrence from those with no recurrence.

Construction and evaluation of the nomogram

As shown in Fig. 4a radiomics nomogram was constructed combining the Com-RS, FIGO stage, menstruation status,

and location to visualize the predictive performance of the model. The first row represents points, and rows second to fifth represent radiomics signature, FIGO stage, menstruation status, and location, respectively. The risk of recurrence of HGSOC is read from the last row of the scale by vertically drawing a line from the total points. Figure 4b and c is calibration curves, showing differences between predicted probabilities of our nomogram and actual values. The closer red-dotted line to the blue solid line indicate the better the performance of nomogram. Our nomogram model has better predictive performance in the training and validation cohort. Comparisons of the Com-RS, clinical model and nomogram are summarized in Table 4. The predictive performance of Com-RS is generally improved with the addition of clinical factors. AUCs of the nomogram reached 0.901 and 0.818 in the training and validation set, respectively, which were higher than those of Com-RS and clinical model. The results of Delong test showed that there were significant differences ($P < 0.05$) between the clinical model and Com-RS and

Table 3 Predictive performance of each radiomics model

Model	Training set					Validation set				
	AUC (95% CI)	ACC	SEN	SPE	P	AUC (95% CI)	ACC	SEN	SPE	P
Intra-RS	0.861 (0.778–0.943)	0.757	0.810	0.750		0.788 (0.633–0.941)	0.694	0.867	0.800	
Peri-RS	0.836 (0.744–0.928)	0.736	0.846	0.743		0.762 (0.582–0.941)	0.722	0.829	0.700	
Com-RS	0.899 (0.831–0.966)	0.811	0.774	0.884		0.815 (0.668–0.962)	0.722	0.929	0.682	
Intra-RS vs. Peri-RS					0.697					0.832
Intra-RS vs. Com-RS					0.486					0.800
Peri-RS vs. Com-RS					0.283					0.653

AUC area under the receiver operating characteristic curve, *CI* confidence interval, *ACC* accuracy; SEN: sensitivity, *SPE* specificity, *Intra-RS* intratumoral radiomics signature, *Peri-RS* peritumoral radiomics signature, *Com-RS* combined radiomics signature

*P < 0.05
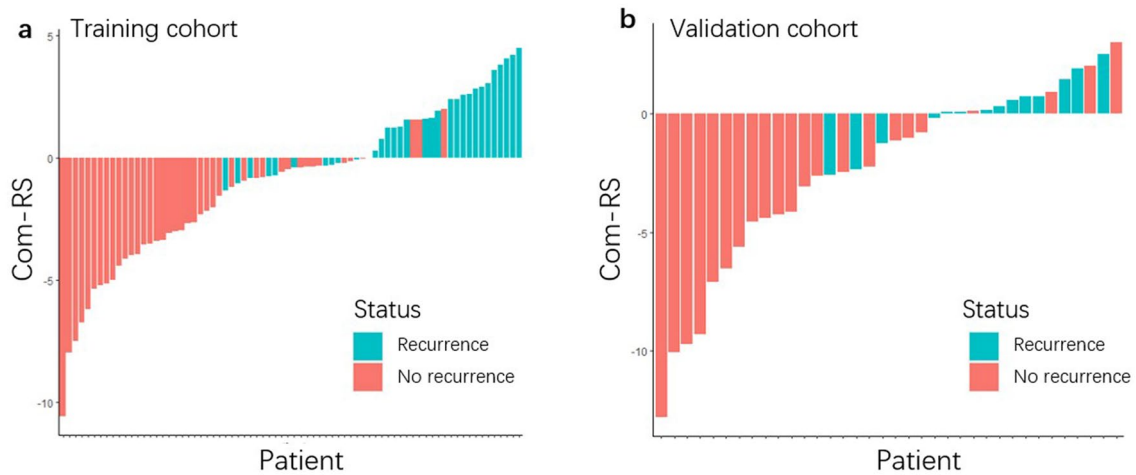
Fig. 3 Waterfall diagram analysis of the developed Com-RS. The Com-RSs for each patient is represented by colored bars. Red bars indicate patients without recurrent cancer, whereas blue bars indi-cate patients with recurrent cancer. The x-axis represents the patient, whereas y-axis represents the Con-RS of each patient

between the clinical model and nomogram, in the training set.

ROC curves for the three radiomics models are plotted in Fig. 5. DCA curves (Fig. 6) represent the potential for clinical application of each model. With a threshold probability range of 0.58–0.80, the red line is higher than the other lines which represents a greater net benefit in our nomogram predicting disease recurrence.

Discussion

Previous reports related to our research focused solely within the extent of the HGSOC tumor itself [11–13, 15], which ignored information from areas surrounding the tumor. We evaluated and compared predictive values of intratumoral and peritumoral regions and found that the established Intra-RS derived from intratumoral area showed higher predictive performance than Peri-RS from peritumoral area in terms of AUC and specificity, suggesting the intratumoral area is more predictive than peritumoral area in HGSOC. Our findings suggested that peritumoral area of HGSOC can provide complementary information correlated with cancer recurrence. This was partially consistent some studies that demonstrated values of peritumoral area for predicting recurrence in malignant tumors [19, 20].

For each patient, the amount of imaging features analyzed in our study was much greater than published studies [11, 13]. We finally selected a total of six features that were highly associated with tumor recurrence, four of which were derived from intratumoral area and two were from peritumoral area. These features included one first-order statistics feature, one gray-level co-occurrence matrix (GLCM) feature, three gray-level size zone (GLSZM) features, and one shape feature (3D). Our findings regarding the association between the four types of features and cancer recurrence were supported by some previous studies [11, 13, 15]. The first-order statistics features quantify the distribution of voxel-based intensities in the tumor [13]. Four textural features (one GLCM feature and three GLSZM features) allow objective and quantitative assessments of tumor heterogeneity [30]. This was consistent with a previous study that suggested the heterogeneity represents a key feature of HGSOC regarding tumor recurrence [31]. The original shape flatness feature quantifies relationship between the largest and smallest principal components in the ROI shape. We found that values of this feature in the non-recurrent group were greater than those in the recurrent group, which may indicate that the tumor with a rounder shape is more tend to recurrent after treatment.

We identified FIGO stage, menopausal status, and tumor location to be the most predictive on recurrent HGSOC by statistical analysis. This was consistent with some previous researches that also considered the three factors (FIGO stage [11, 13, 15], menopausal [11] and location [12] as high-risk clinical factors for recurrent HGSOC. Although the CA125 was considered to be an important clinical predictor according to previous reports [11, 15], we found no difference for CA125 ($P > 0.05$) in the validation set, which may be due to the limited sample size. By integrating the FIGO stage, menopausal status, and tumor location, we built a clinical model and generated predictive AUCs ranging from 0.648 to 0.666, which was similar with recently proposed clinical models that yielded AUCs of 0.632–0.691) [13] and 0.670–0.670 [12] for predicting recurrent HGSOC. To help clinicians visualize predictive
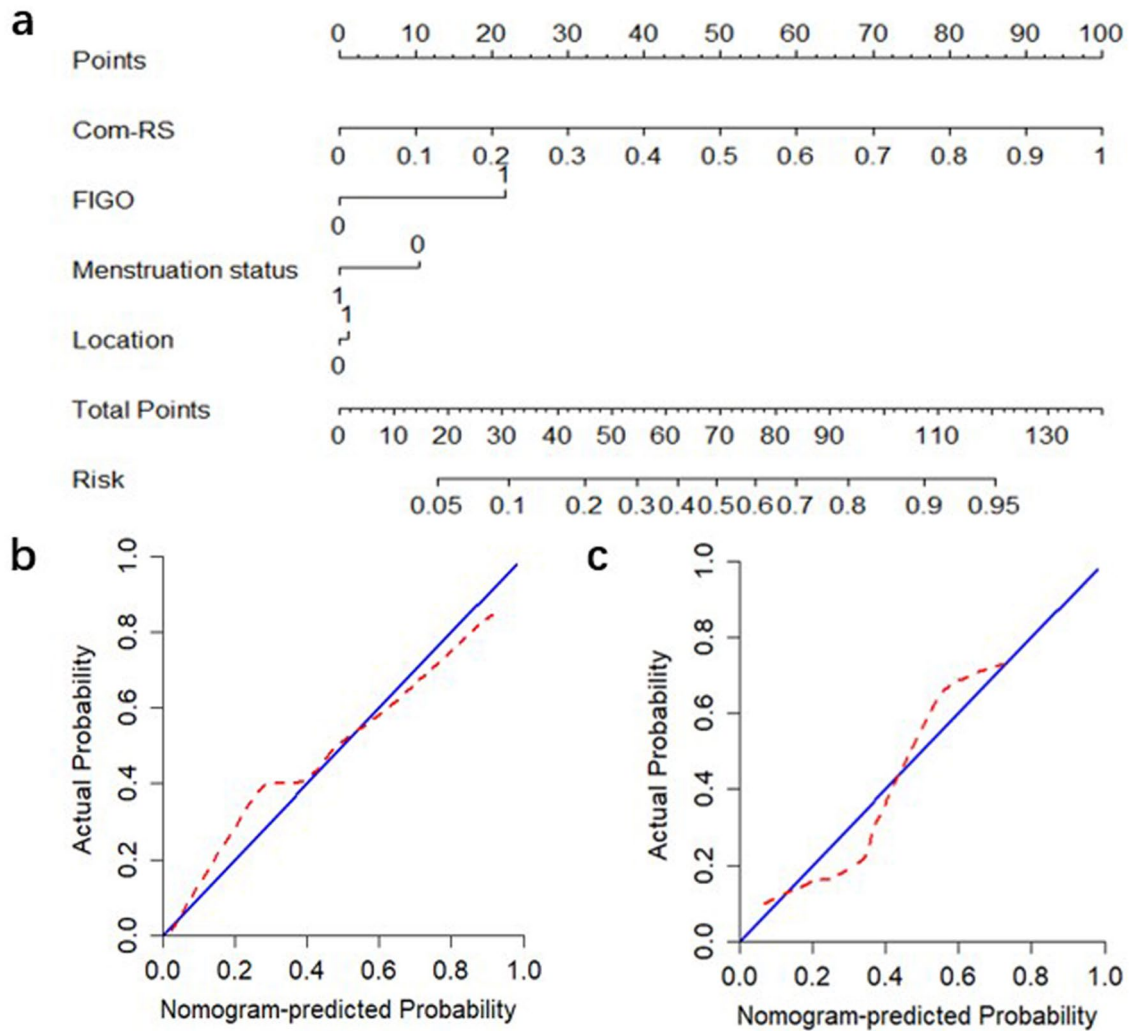
Fig. 4 Radiomics nomogram combining the Com-RS and important clinical factors. **a** The developed nomogram. **b** and **c** Calibration curves of the nomogram in the training (**b**) and validation (**c**) cohort. The x-axis represents the model calculated, whereas y-axis represents the actual probabilities. The 45 degree blue line represents an ideal diagnosis, whereas red-dotted line represent the performance of our nomogram

Table 4 Comparisons of the Com-RS, clinical model, and nomogram

| Model	Training set					Validation set				
	AUC (95% CI)	ACC	SEN	SPE	P	AUC (95% CI)	ACC	SEN	SPE	P
M1	0.899 (0.831–0.966)	0.811	0.774	0.884		0.815 (0.668–0.962)	0.722	0.929	0.682	
M2	0.648 (0.527–0.769)	0.581	0.710	0.512		0.666 (0.582–0.941)	0.611	0.786	0.500	
M3	0.901 (0.835–0.967)	0.824	0.806	0.837		0.818 (0.499–0.833)	0.694	0.786	0.818	
M1 vs. M2					<0.001*					0.160
M1 vs. M3					0.890					0.878
M2 vs. M3					<0.001*					0.114

AUC area under the receiver operating characteristic curve, *CI* confidence interval, *ACC* accuracy, *SEN* sensitivity, *SPE* specificity, *M1* Com-RS, *M2* clinical model, *M3* nomogram

*$P < 0.05$
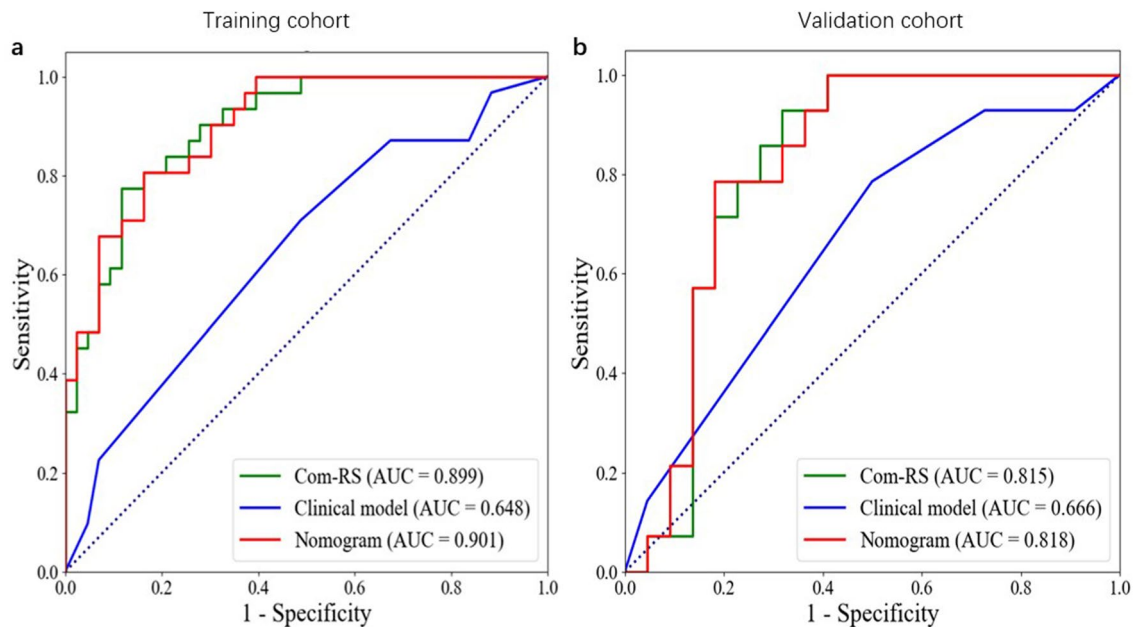
Fig. 5 ROC curves of Com-RS, clinical model, and nomogram in the training (**a**) and validation (**b**) cohort
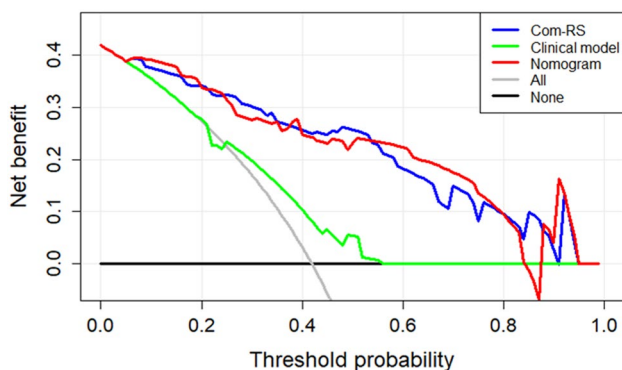
Fig. 6 DCA curves for the developed Com-RS, clinical model, and nomogram. The x-axis represents threshold probability for the patients, whereas the y-axis represents net benefits. The black line represent the hypothesis that all patients were without recurrent cancer. The gray line represents the assumption that all patients were with recurrent cancer. The red, blue, and green lines represent the nomogram, Com-RS, and clinical model, respectively

risks of tumor recurrence in HGSOC patients, an easy-to-use radiomics-clinical nomogram was constructed incorporating image-based features and high-risk clinical factors. Compared to Com-RS and clinical model, our nomogram had the best prediction performance and generated AUCs of 0.818–0.901, which were much higher than a previous report yielded AUCs of 0.749–0.769 [13]. DCA confirms that more benefits can be provided by our nomogram, which suggested good potential in clinical applications.

There are some limitations in this study. First, the HGSOC patients were enrolled from a single hospital. The findings should be validated with multicenter samples. Second, we only analyzed CT data. While, a previous study showed that PET-CT may be more powerful for assessment of cancer recurrence in HGSOC compared to CT [32]. Third, due to incomplete records of genotypes for the patients, this study failed to explore associations between gene status and cancer recurrence. Fourth, although peritumoral dilations were automatically addressed, intratumoral regions were manually segmented, which was subjective and time consuming. Therefore, automated or semi-automated methods for tumor segmentation are needed in our future study. Finally, our study included a peritumoral area with a dilatation distance of 1 cm. In our future studies, performance of different dilatation distances should be evaluated.

Conclusion

This study investigated values of intra- and peritumoral regions of ovarian cancer for predicting cancer recurrence. Our constructed clinical-radiomics nomogram may be of potential significance for making early and appropriate treatment decisions in patients with HGSOC.

Declarations

Conflict of interest The authors declare that they have no conflict of interest.

Consent for publication Not applicable.

References

1. [1] Lee SJ, Kay CS, Kim YS, Son SH, Kim M, Lee SW, et al (2019) Ovarian cancer: Current status and strategies for improving therapeutic outcomes. Cancer Med 8(4):7018-7031. https://doi.org/https://doi.org/10.3857/roj.2017.00115

2. [2] Kroeger PT Jr, Drapkin R (2017) Pathogenesis and heterogeneity of ovarian cancer. Curr Opin Obstet Gynecol 29(1):26-34. https://doi.org/https://doi.org/10.1097/gco.0000000000000340

3. [3] Stewart C, Ralyea C, Lockwood S (2019) Ovarian Cancer: An Integrated Review. Semin Oncol Nurs 35:151-156.

4. [4] Siegel RL, Miller KD, Jemal, A (2020) Cancer statistics, 2020. CA Cancer J. Clin 70(2):7-30. https://doi.org/https://doi.org/10.1016/j.soncn.2019.02.001

5. [5] Zhu H, Ai Y, Zhang J, Zhang J, Jin J, Xie C et al (2021) Preoperative Nomogram for Differentiation of Histological Subtypes in Ovarian Cancer Based on Computer Tomography Radiomics. Front Oncol 11:642892. https://doi.org/https://doi.org/10.3389/fonc.2021.642892

6. [6] Wei W, Rong Y, Liu Z, Zhou B, Tang Z, Wang S et al (2018) Radiomics: a Novel CT-Based Method of Predicting Postoperative Recurrence in Ovarian Cancer. Annu Int Conf IEEE Eng Med Biol Soc 2018:4130-4133. https://doi.org/https://doi.org/10.1109/embc.2018.8513351

7. [7] Manganaro L, Gigli S, Antonelli A, Saldari M, Tomao F, Marchetti C et al (2019) Imaging strategy in recurrent ovarian cancer: a practical review. Abdom Radiol (NY) 44(3):1091-1102. https://doi.org/https://doi.org/10.1007/s00261-018-1677-y

8. [8] Nougaret S, McCague C, Tibermacine H, Vargas HA, Rizzo S, Sala E (2021) Radiomics and radiogenomics in ovarian cancer: a literature review. Abdom Radiol (NY) 46(6):2308-2322. https://doi.org/https://doi.org/10.1007/s00261-020-02820-z

9. [9] Lambin P, Leijenaar RTH, Deist TM, Peerlings J, de Jong EEC, van Timmeren J et al (2017) Radiomics: the bridge between medical imaging and personalized medicine. Nat Rev Clin Oncol 14(12):749-762. https://doi.org/https://doi.org/10.1038/nrclinonc.2017.141

10. [10] Guiot J, Vaidyanathan A, Deprez L, Zerka F, Danthine D, Frix AN et al (2022) A review in radiomics: Making personalized medicine a reality via routine imaging. Med Res Rev 42(1):426-440. https://doi.org/https://doi.org/10.1002/med.21846

11. [11] Wei W, Liu Z, Rong Y, Zhou B, Bai Y, Wei W et al (2019) A Computed Tomography-Based Radiomic Prognostic Marker of Advanced High-Grade Serous Ovarian Cancer Recurrence: A Multicenter Study. Front Oncol. 9:255. https://doi.org/https://doi.org/10.3389/fonc.2019.00255

12. [12] Wang X, Lu Z (2021) Radiomics Analysis of PET and CT Components of 18F-FDG PET/CT Imaging for Prediction of Progression-Free Survival in Advanced High-Grade Serous Ovarian Cancer. Front Oncol 11:638124. https://doi.org/https://doi.org/10.3389/fonc.2021.638124

13. [13] Chen HZ, Wang XR, Zhao FM, Chen XJ, Li XS, Ning G et al (2021) A CT-based radiomics nomogram for predicting early recurrence in patients with high-grade serous ovarian cancer. Eur J Radiol 45:110018. https://doi.org/https://doi.org/10.1016/j.ejrad.2021.110018

14. [14] Li HM, Gong J, Li RM, Xiao ZB, Qiang JW, Peng WJ et al (2021) Development of MRI-Based Radiomics Model to Predict the Risk of Recurrence in Patients With Advanced High-Grade Serous Ovarian Carcinoma. AJR Am J Roentgenol 217(3):664-675. https://doi.org/https://doi.org/10.2214/ajr.20.23195

15. [15] Rizzo S, Botta F, Raimondi S, Origgi D, Buscarino V, Colarieti A et al (2018) Radiomics of high-grade serous ovarian cancer: association between quantitative CT features, residual tumour and disease progression within 12 months. Eur Radiol 28(11):4849-4859. https://doi.org/https://doi.org/10.1007/s00330-018-5389-z

16. [16] Cobec IM, Sas I, Pirtea L, Cimpean AM, Moatar AE, Ceauşu RA et al (2016) Podoplanin as Key Player of Tumor Progression and Lymph Vessel Proliferation in Ovarian Cancer. Anticancer Res 36(10):5265-5272. https://doi.org/https://doi.org/10.21873/anticanres.11097

17. [17] Ween MP, Oehler MK, Ricciardelli C (2011) Role of versican, hyaluronan and CD44 in ovarian cancer metastasis. Int J Mol Sci 12(2):1009-29. https://doi.org/https://doi.org/10.3390/ijms12021009

18. [18] Akinci D'Antonoli T, Farchione A, Lenkowicz J, Chiappetta M, Cicchetti G, Martino A et al (2020) CT Radiomics Signature of Tumor and Peritumoral Lung Parenchyma to Predict Nonsmall Cell Lung Cancer Postsurgical Recurrence Risk. Acad Radiol 27(4):497-507. https://doi.org/https://doi.org/10.1016/j.acra.2019.05.019

19. [19] Xu L, Wan Y, Luo C, Yang J, Yang P, Chen F et al (2021) Integrating intratumoral and peritumoral features to predict tumor recurrence in intrahepatic cholangiocarcinoma. Phys Med Biol 66(12). https://doi.org/https://doi.org/10.1088/1361-6560/ac01f3

20. [20] Ahn H, Won Lee J, Jang SH, Ju Lee H, Lee JH, Oh MH et al (2021) Prognostic significance of imaging features of peritumoral adipose tissue in FDG PET/CT of patients with colorectal cancer. Eur J Radiol 145:110047. https://doi.org/https://doi.org/10.1016/j.ejrad.2021.110047

21. [21] van Griethuysen JJM, Fedorov A, Parmar C, Hosny A, Aucoin N, Narayan V et al (2017) Computational Radiomics System to Decode the Radiographic Phenotype. Cancer Res 77(21):e104-e107. https://doi.org/https://doi.org/10.1158/0008-5472.can-17-0339

22. [22] Koo TK, Li MY (2016) A guideline of selecting and reporting intra-class correlation coefficients for reliability research. J Chiropr Med 15:155-163

23. [23] Sauerbrei W, Royston P, Binder H (2007) Selection of important variables and determination of functional form for continuous predictors in multivariable model building. Stat Med 26(30):5512-28. https://doi.org/https://doi.org/10.1002/sim.3148

24. [24] Robert T (2011) Regression shrinkage and selection via the lasso: a retrospective. J R Stat Soc Ser B Stat Methodol 73:267–288.

25. [25] McHugh ML (2013) The chi-square test of independence. Biochem Med (Zagreb) 23(2):143-9. https://doi.org/https://doi.org/10.11613/bm.2013.018

26. [26] Roman H (2009) Tests statistiques utilisés en médecine. Test non paramétrique de Mann et Whitney [Statistics in medicine:

Mann and Whitney test]. Gynecol Obstet Fertil 37(2):208-9. https://doi.org/https://doi.org/10.1016/j.gyobfe.2009.01.002

27. [27] Ruopp MD, Perkins NJ, Whitcomb BW et al (2008) Youden index and optimal cut-point estimated from observations affected by a lower limit of detection. Biom J 50(3):419–430. https://doi.org/https://doi.org/10.1002/bimj.200710415

28. [28] DeLong ER, DeLong DM, Clarke-Pearson DL (1988) Comparing the areas under two or more correlated receiver operating characteristic curves: a nonparametric approach. Biometrics 44(3):837–845

29. [29] Vickers AJ, Elkin EB (2006) Decision Curve Analysis: A Novel Method for Evaluating Prediction Models. Med Decis Making 26(6):565–74. https://doi.org/https://doi.org/10.1177/0272989x06295361

30. [30] Lubner MG, Smith AD, Sandrasegaran K et al (2017) CT Texture Analysis: Definitions, Applications, Biologic Correlates, and Challenges. Radiographics. 37(5):1483-1503. https://doi.org/https://doi.org/10.1148/rg.2017170056

31. [31] Kossaï M, Leary A, Scoazec JY et al (2018) Ovarian Cancer: A Heterogeneous Disease. Pathobiology 85(1-2):41-49. https://doi.org/https://doi.org/10.1159/000479006

32. [32] Hornung R, Urs E, Serenella E, Edward W, Ursula S, Urs H et al (2004) Analysis of potential prognostic factors in 111 patients with ovarian cancer. Cancer Lett 206(1):97-106. https://doi.org/https://doi.org/10.1016/j.canlet.2003.10.034